01 Jul 2017

# Analysis Of Time-dependent Bearing Capacity Of A Driven Pile In Clayey Soils By Total Stress Method

Lin Li

Jingpei Li

De'an Sun

Weibing Gong
*Missouri University of Science and Technology*, weibing.gong@mst.edu



## Recommended Citation

L. Li et al., "Analysis Of Time-dependent Bearing Capacity Of A Driven Pile In Clayey Soils By Total Stress Method," *International Journal of Geomechanics*, vol. 17, no. 7, article no. 04016156, American Society of Civil Engineers, Jul 2017.
The definitive version is available at https://doi.org/10.1061/(ASCE)GM.1943-5622.0000860

# Analysis of Time-Dependent Bearing Capacity of a Driven Pile in Clayey Soils by Total Stress Method

Lin Li[1]; Jingpei Li[2]; De'an Sun[3]; and Weibing Gong[4]

**Abstract:** This paper proposes an analytical approach to evaluate the time-dependent bearing capacity of a driven pile in clayey soils by taking the pile installation and subsequent reconsolidation effects into consideration. The process of pile installation is modeled by undrained expansion of a spherical cavity at the pile tip and a cylindrical cavity around the pile shaft. The cavity expansion solution, which is based on a $K_0$-consolidated anisotropic modified Cam-clay model ($K_0$-AMCC), is used to capture the pile installation effects. After pile installation, the dissipation of the excess pore water and the increase of the effective stress in the surrounding soil are evaluated by the radial consolidation theory. Based on the effective stress, the strength of the remolded soil is quantified by the modified Cam-clay (MCC) model and the spatially mobilized plane (SMP) criterion. With the three-dimensional strength of the surrounding soil, the time-dependent bearing capacity of the driven pile is evaluated by the total stress ($\alpha$) method. To verify the proposed analytical approach, three groups of centrifuge model tests were performed, and the proposed approach was applied to predict the time-dependent bearing capacity of the tested piles. It is shown that reasonable predictions can be made by the method proposed in this paper. **DOI: 10.1061/(ASCE)GM.1943-5622.0000860.** 

**Author keywords:** Driven pile; Anisotropic; Stress history; Time-dependent bearing capacity; Centrifuge model tests.

## Introduction

When a pile is driven into saturated clay, stresses in the surrounding soil change significantly. Large displacement, large strains, and high excess pore-water pressure are formed in the soil adjacent to the pile (Pestana et al. 2002; Abu-Farsakh et al. 2015). After pile installation, the excess pore-water pressure dissipates and the surrounding disturbed soil regains its strength, which results in setup effects on the bearing capacity of driven piles (Konrad and Roy 1987; Skov and Denver 1988). Generally, driven piles in clay tend to experience longer-term setup than piles in sand, and the setup effects have a significant impact on determining the pile capacity (Basu et al. 2014). However, it is difficult to quantify the stress state of the surrounding soil, because the complex stress-strain changes occur during pile installation, equalization, and load testing. Consequently, modeling of the time-dependent bearing capacity of driven piles through an analytical approach is problematic.

Many researchers have developed empirical approaches to predict the capacity of a driven pile in clayey soils through field and laboratory testing as well as a cone penetration test (CPT) and piezocone penetration test (CPTU) (Skov and Denver 1988; Bond and Jardine 1991; Lehane and Jardine 1994; Eslami and Fellenius 1997; Yang and Liang 2006; Ng et al. 2013; Mohamed and El Naggar 2015). In particular, the semilogarithmic empirical relationship, proposed by Skov and Denver (1988), has been widely used to predict the postinstallation increase in pile capacity with time. However, many of these approaches had limitations because they were developed for specific geological conditions. Apart from empirical approaches, several researchers attempted to study the setup effect of driven piles in clay by finite-element analysis (Mabsout and Sadek 2003; Livneh and El Naggar 2008; Chakraborty and Kumar 2013; Elsherbiny and El Naggar 2013; Fakharian et al. 2014; Basu et al. 2014; Abu-Farsakh et al. 2015). With the FEM, the setup effects can be properly modeled because many complicated factors can be incorporated into the numerical model. Nonetheless, its application is limited in practice because of the complicated modeling process and high computational requirements.

With an accumulation of experience and knowledge on the setup phenomenon, some researchers have attempted to incorporate the setup effects into the analytical approach to determine the bearing capacity of driven piles (Vesic 1973; Randolph and Wroth 1979; Coop and Wroth 1990; El Naggar and Novak 1992; Guo 2000; Yu 2000; Veiskarami et al. 2011; Randolph 2003; Qi et al. 2015). However, in most of these studies, the in situ stress was assumed to be isotropic, and the strength of the soil adjacent to the pile during pile loading was evaluated by ignoring the three-dimensional strength property. It is well known that the in situ anisotropic stress of natural clay has significant effects on the mechanical behaviors of soil, and the soil exhibits three-dimensional strength property during shearing (Sekiguchi and Ohta 1977; Matsuoka et al. 1999). Moreover, the majority of the previous studies only focused on the effects of pile installation or subsequent consolidation (Basu et al. 2014). A thorough analytical method or a general form formula for the time-dependent bearing capacity is not currently available.

The main aim of this paper is to present a complete analytical approach to evaluate the time-dependent bearing capacity of a driven pile in saturated anisotropic natural clay. For this, some previous solutions and procedures for the pile installation and

[1]Ph.D. Student, Dept. of Geotechnical Engineering, Tongji Univ., Shanghai 200092, China. E-mail: lilin_sanmao@163.com

[2]Professor, Dept. of Geotechnical Engineering, Tongji Univ., Shanghai 200092, China (corresponding author). E-mail: lijp2773@163.com

[3]Professor, Dept. of Civil Engineering, Shanghai Univ., Shanghai 200444, China. E-mail: sundean06@163.com

[4]Master's Degree Candidate, Dept. of Geotechnical Engineering, Tongji Univ., Shanghai 200092, China. E-mail: weibingthomas@163.com

Note. This manuscript was submitted on June 27, 2016; approved on October 13, 2016; published online on December 5, 2016. Discussion period open until May 5, 2017; separate discussions must be submitted for individual papers. This paper is part of the ***International Journal of Geomechanics***, © ASCE, ISSN 1532-3641.

subsequent consolidation are integrated and developed to a set of equations for the time-dependent capacity of a driven pile in terms of the total stress method (referred to as the $\alpha$ method). The in situ stress history of the natural clay, the pile installation effect, the subsequent consolidation, and the three-dimensional strength property of the surrounding soil during pile loading, all of which have pronounced effects on the bearing capacity of a driven pile, are reasonably considered in the proposed approach. Three groups of centrifuge model tests were performed, and the test results were predicted by the proposed approach to demonstrate its validity and reliability. Some time-dependent bearing capacity factors are then presented for a driven pile in clayey soils with different in situ stress histories, and the effects of the in situ anisotropic stress and the overconsolidation ratio (OCR) on these factors are also investigated.

## Modeling and Analysis of Pile Installation in Saturated Natural Clays

During pile installation, the surrounding soil will be displaced predominantly outward, with strain fields resembling spherical cavity expansion ahead of the pile tip and cylindrical cavity expansion along the pile shaft (Randolph 2003). Although the process of pile installation is neither strictly a spherical cavity expansion nor a cylindrical cavity expansion, a number of previous studies showed that the stress state of the soil around a driven pile can be modeled by the cavity expansion theory with sufficient accuracy (Butterfield and Banerjee 1970; Guo 2000). Therefore, to analyze the problem analytically, the pile installation process is modeled as an undrained expansion of a spherical cavity at the pile tip and a cylindrical cavity around the pile shaft in this study. Fig. 1 shows schematically cavity expansion models for pile installation in $K_0$-consolidated saturated natural clay. The in situ effective horizontal stress $\sigma'_{h0}$ is equal to the product of vertical stress $\sigma'_{v0}$ and coefficient of earth pressure at rest $K_0$. The coefficient $K_0$ describes the degree of the anisotropy of the initial stresses. As the pile is driven in, a cavity is created that gradually expands from its initial zero radius $r_0$ to the pile radius $r_d$. During this process high excess pore-water pressure is generated, and a plastic region is formed in the surrounding soil.

Li et al. (2016) presented an analytical solution for the undrained expansion of a cylindrical cavity in $K_0$-consolidated anisotropic natural clays. A $K_0$-consolidated anisotropic modified Cam-clay ($K_0$-AMCC) model and logarithmic strains were used in the solution to consider the in situ anisotropic stress and large deformation effects. Using this solution, the pile installation effect on the soil around the pile shaft can be evaluated. For spherical cavity expansion, the isotropic assumption is essential for obtaining an analytical solution, because the derivation has to be conducted under the spherical symmetry condition. To assess the pile installation effect on the soil around the pile tip, it is approximately assumed that the three in situ normal stresses around the pile tip are all equal to the mean effective stress, $p'_o$ ($= a'_{\mathrm{iio}}/3$) (i.e., $K_0 = 1$). Based on this assumption, the installation effect on the soil around the pile tip can be captured by the modified Cam-clay (MCC) model-based solution for the undrained expansion of a spherical cavity, which was proposed by Cao et al. (2001). Following Li et al. (2016) and Cao et al. (2001), the expression for the distribution of excess pore pressure $u_{e0}$ in the surrounding plastic region, induced by the pile installation, can be written in a single equation as follows:

$$u_{e0} = p'_0\left(\frac{3K_0}{1+2K_0}+\frac{m\eta^*_p}{\sqrt{3^m}}\right) + p'_f\left(\sqrt{3^{m-1}}\varsigma\ln\frac{r_p}{r}-\frac{\varsigma}{2^{2-m}\sqrt{3^{m-1}}}\pm\frac{\sqrt{4M^2-3\varsigma^2}}{6}-1\right) \tag{1}$$

where $m = 1$ and $m = 2$ indicate the cylindrical case (Li et al. 2016) and the spherical case (Cao et al. 2001), respectively. The plus sign is taken when $K_0 \le 1$; conversely, the minus sign is taken when $K_0 > 1$. The expressions of the slope of the critical state line $M$, the relative stress ratio at the elastic-plastic (EP) boundary $\eta^*_p$, the plastic radius $r_p$, the ultimate mean stress $p'_f$ in the soil adjacent to the pile, and the parameter $\varsigma$ can be given, respectively, as follows:

$$M = \frac{6\sin\phi'}{3-\sin\phi'} \tag{2}$$

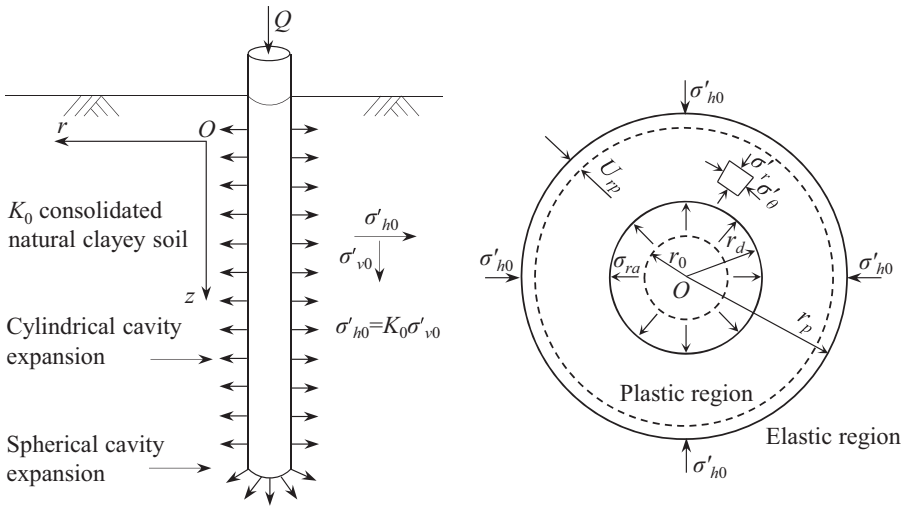


**Fig. 1.** Cavity expansion model for pile installation in natural saturated clay

$$\eta_p^* = M^* \sqrt{\mathrm{OCR} - 1} \tag{3}$$

$$\left(\frac{r_p}{r_d}\right)^{m+1} = \frac{2mG}{(m+1)\left(\sigma'_{\mathrm{rp}} - \sigma'_{ho}\right)} \tag{4}$$

$$p'_f = p'_0 \left(\frac{\mathrm{OCR}}{2}\right)^{\Lambda} \tag{5}$$

$$s = \frac{2\sqrt{3\left[M^2(2K_0+1)^2 - 9(1-K_0)^2\right]}}{3(2K_0+1)} \tag{6}$$

where $\sigma'_{\mathrm{rp}} = \sigma'_{h0} + mp'_0\eta_p^*/\sqrt{3^m}$ is the radial effective stress at the EP boundary; and $\phi'$ = effective internal friction angle. The shear modulus $G$, the plastic volumetric strain ratio $\Lambda$, and the relative stress ratio at critical state $M^*$ are defined, respectively, as follows:

$$G = \frac{3(1-2\nu')vp'}{2(1+\nu')\kappa} \tag{7}$$

$$M^* = \sqrt{M^2 - \eta_0^2} \tag{8}$$

$$\Lambda = 1 - \frac{\kappa}{\lambda} \tag{9}$$

where $\kappa$ and $\lambda$ = slope of swelling line and loading line, respectively; $v$ = specific volume; and $\nu'$ = effective Poisson's ratio. The initial stress ratio $\eta_0$ is defined as

$$\eta_0 = \left|\frac{3(1-K_0)}{2K_0+1}\right| \tag{10}$$

Based on Eqs. (1) and (5), one can evaluate the stress states of the soil adjacent to the pile immediately after pile installation. The stress conditions will be applied to analyze the subsequent consolidation in the following section.

## Consolidation after Pile Installation

### *Dissipation of Excess Pore-Water Pressure*

After pile installation, field measurements showed that excess pore-water pressure dissipates predominantly in the radial direction (Roy et al. 1981; Guo 2000). Thus, it can be assumed that consolidation takes place primarily by the radial flow of pore water. According to Randolph and Wroth (1979), the governing equation for radial consolidation can be given as follows:

$$C_h \nabla^2 u_e = \frac{\partial u_e}{\partial t} \tag{11}$$

where

$$\nabla^2 = \frac{\partial^2}{\partial r^2} + \frac{1}{r}\frac{\partial}{\partial r} \tag{12}$$

where $C_h$ = coefficient of consolidation for radial horizontal drainage, given by

$$C_h = \frac{k_h}{\gamma_w}\frac{2(1-\nu')G}{1-2\nu'} \tag{13}$$

where $k_h$ = horizontal coefficient of permeability; and $\gamma_w$ = unit weight of water.

Following Randolph and Wroth (1979), the general solution of Eq. (11) can be obtained by the variable separation method as follows:

$$u_e = \sum_{n=1}^{\infty} C_{1n}[J_0(\lambda_n r) + C_{2n}Y_0(\lambda_n r)]e^{-\lambda_n^2 C_h t} \tag{14}$$

where $J_0$ and $Y_0$ = zero-order Bessel functions of the first and second kind, respectively; $\lambda_n$ = eigenvalue of the Bessel function; and $C_{1n}$ and $C_{2n}$ = integration constants.

For impermeable piles, the boundary and initial conditions for Eq. (11) can be given as follows:

$$\left.\frac{\partial u_e}{\partial r}\right|_{r=r_d} = 0 \ (t \geq 0) \tag{15}$$

$$u_e|_{r=R} = 0 \ (t \geq 0) \tag{16}$$

$$u_e|_{t=0} = u_{e0} \ (t = 0, r \geq r_d) \tag{17}$$

where $R$ = radius beyond which the excess pore-water pressure can be negligible at any time. Generally, the value of $R$ can be taken as 5–10 times plastic radius $r_p$. (Guo 2000).

Making use of Eqs. (15)–(17), the value of $\lambda_n$, $C_{1n}$, and $C_{2n}$ can be determined as

$$Y_0(\lambda_n R)J_1(\lambda_n r_d) - J_0(\lambda_n R)Y_1(\lambda_n r_d) = 0 \tag{18}$$

$$C_{1n} = \frac{\int_{r_d}^{R} u_{e0}\left[J_0(\lambda_n r) - \frac{J_0(\lambda_n R)}{Y_0(\lambda_n R)}Y_0(\lambda_n r)\right] rdr}{\int_{r_d}^{R}\left[J_0(\lambda_n r) - \frac{J_0(\lambda_n R)}{Y_0(\lambda_n R)}Y_0(\lambda_n r)\right]^2 rdr} \tag{19}$$

$$C_{2n} = -\frac{J_0(\lambda_n R)}{Y_0(\lambda_n R)} \tag{20}$$

### *Evolution of Mechanical Behaviors of the Surrounding Soil*

With dissipation of the excess pore-water pressure, the disturbed surrounding soil regains strength due to the increase of the effective stress. According to the one-dimensional radial consolidation theory, the increment of the mean effective stress $\delta p'$ (where $\delta p' = (\delta\sigma'_r + \delta\sigma'_\theta + \delta\sigma'_z)/3$) under the plane strain condition can be expressed as (Randolph and Wroth 1979)

$$\delta p' = \frac{1+v'}{3(1-v')}[u_{e0} - u_e] \tag{21}$$

Hence, the mean effective stress, $p'(t)$, in the soil adjacent to the pile after pile installation can be given as

$$p'(t) = p'_f + \frac{1+v'}{3(1-v')}[u_{e0} - u_e] \tag{22}$$

During pile installation, the soil adjacent to the pile undergoes severe distortion and change in the fabric, leading to two major remolding effects on the surrounding soil: erasing the stress history and collapsing the soil structure. After pile installation, the surrounding remolded soil exhibits mechanical behaviors similar to the normally consolidated clay (Randolph and Wroth 1981). Therefore, based on the MCC model, the in situ and the remolded undrained shear strength $s_{u0tc}$ and $s_{utc}(t)$ of the surrounding soil in terms of triaxial compression can be expressed, respectively, as follows:

$$s_{u0tc} = \frac{1}{2}q_{0f} = \frac{1}{2}Mp'_0\left(\frac{OCR}{2}\right)^{\Lambda} \tag{23}$$

$$s_{utc}(t) = \frac{1}{2}q_f(t) = \frac{1}{2}Mp'(t)\left(\frac{1}{2}\right)^{\Lambda} \tag{24}$$

where $q_{0f}$ and $q_f(t)$ = ultimate deviate stresses under triaxial compression condition for the in situ and the remolded soil, respectively.

Eqs. (22) and (24) demonstrate that the strength of the surrounding soil increases with the increase of the mean effective stress $p'(t)$ due to dissipation of the excess pore-water pressure, which well explains the primary cause for the time-dependent bearing capacity and setup effect of driven piles after installation.

## Determination of Axial Bearing Capacity of Driven Piles

### *Pile Shaft Resistance*

Several methods are available for calculating the unit shaft resistance $f_s$, such as the total stress ($\alpha$) method, the effective stress ($\beta$) method, the CPTU method, and other empirical methods. Among these methods, the effective stress method, which relates $f_s$ to radial effective stress at failure and interface friction angle via in situ effective vertical stress and a parameter $\beta$, is considered to be a rational way to evaluate the shaft resistance. However, the parameters involved in the effective stress method are difficult to determine, because the complex stress-strain changes occur at the pile-soil interface during pile installation, subsequent consolidation, and loading processes. Because of its simplicity, the $\alpha$ method remains the most popular approach for estimating the shaft capacity of piles in clay. Hence, the $\alpha$ method will be used to evaluate the shaft resistance in this study.

Based on the $\alpha$ method, the time-dependent unit shaft resistance $f_s(t)$ can be determined by

$$f_s(t) = \alpha(t)s_{u0tc} \tag{25}$$

where $\alpha(t)$ is the time-dependent pile shaft resistance factor and will be determined in subsequent discussions.

When a pile is subjected to axial compressive load, the model of shearing of the soil around the pile shaft is very similar to that in a simple shear test, and the failure stress in a simple shear test can be related to the undrained shear stress measured in triaxial compression tests (Randolph and Wroth 1981). Therefore, it is possible to develop an analytical approach to determine the coefficient $\alpha(t)$ based on the undrained shear strength under the triaxial compression condition. As shown in Fig. 2, if it is assumed that the average normal stress $a'_y$ and horizontal stress $a'_x$ acting on the sample in an undrained simple shear test are equal to the radial stress $a'_r$ and vertical stress $a'_v$ acting on the soil element adjacent to the pile shaft, respectively. The failure shear stress $\tau_{yx}$ acting on the top of the sample can then be taken as the unit shaft resistance $f_s$. As shown in Fig. 3, in a simple shear test, the failure envelope will be tangential to the effective stress circle at Point B, whereas the failure stress state on the top face of the sample lies in Point A, giving the geometrical relationship between failure stress $\tau_{yx}$ and Mohr's circle radius $s_{ups}$ as follows:

$$\tau_{yx} = f_s = s_{ups}\cos\phi' \tag{26}$$

where $s_{ups}$ = undrained shear strength under plane strain condition due to the deformation mode of the sample in the simple shear tests.

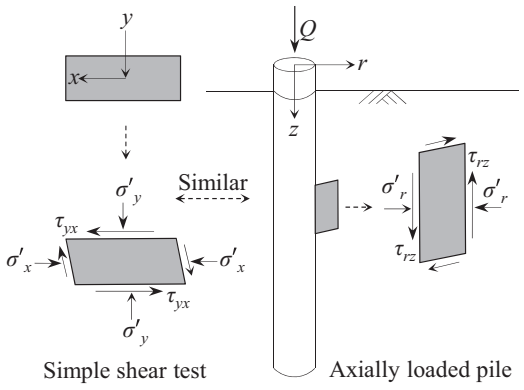


**Fig. 2.** Stress state of the soil near the pile shaft and the soil sample in the simple shear test

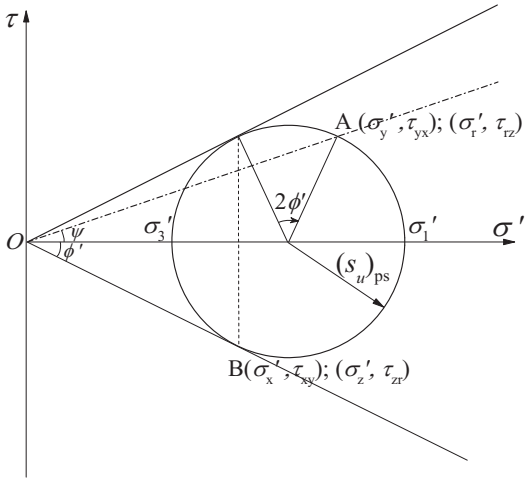


**Fig. 3.** Failure stress state of soil around the pile shaft

The soil exhibits different strength properties under different shear conditions, and the three-dimensional strength of soils can be properly modeled by the spatially mobilized plane (SMP) or Lade's criteria (Matsuoka and Sun 2006). To evaluate the shear strength under the plane strain condition from the strength under the triaxial compression condition, the stress-transformed method (Matsuoka et al. 1999), which proposes a transformed stress tensor $\tilde{\sigma}'_{ij}$ instead of the real stress $\sigma'_{ij}$ to transfer the SMP curve in the $\pi$ plane to become a circle, as shown in Fig. 4, is adopted in this paper. From the geometrical relationship between the Points A and $A'$ in Fig. 4, the undrained shear strength under triaxial compression can be transformed to the strength under plane strain condition as follows:

$$s_{ups} = \frac{3\sqrt{3}\sin\varphi_f}{2M\cos\psi_f\sqrt{2+\sin^2\varphi_f}} s_{utc} \tag{27}$$

where $\varphi_f$ and $\psi_f$ = stress-transformed parameters, which can be given as

$$\sin\varphi_f = \frac{\sqrt{2}M}{\sqrt{9+3M}} \tag{28}$$

$$\psi_f = \frac{1}{3}\cos^{-1}\left\{-\left(\frac{3}{2+\sin^2\varphi_f}\right)^{3/2}\sin\varphi_f\cos 3\theta\right\} \tag{29}$$

with Lode's stress angle $\theta = \pi/6$ under the plane strain condition.

From Eqs. (23) and (24) along with Eqs. (25)–(27), one can obtain

$$f_s(t) = \frac{3\sqrt{3}\sin\varphi_f\cos\phi'}{2M\cos\psi_f\sqrt{2+\sin^2\varphi_f}}\frac{1}{\mathrm{OCR}^{\Lambda}}\frac{p'(t)}{p'_0}s_{utc0} \tag{30}$$

Based on the $\alpha$ method, the time-dependent adhesion coefficient $\alpha(t)$ can then be expressed as

$$\alpha(t) = \frac{3\sqrt{3}\sin\varphi_f\cos\phi'}{2M\cos\psi_f\sqrt{2+\sin^2\varphi_f}}\frac{1}{\mathrm{OCR}^{\Lambda}}\frac{p'(t)}{p'_0} \tag{31}$$

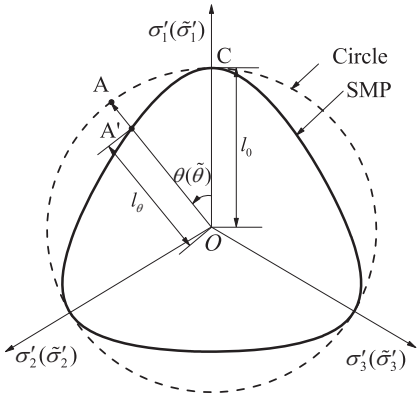


**Fig. 4.** SMP criterion in $\pi$-plane and transformed $\pi$-plane

### Pile End Resistance

For piles in clayey soils, the end bearing capacity is usually much less than the shaft bearing capacity; thus, it is sufficient to evaluate the unit end resistance $q_b$ in terms of the total stress method by the following equation:

$$q_b = N_c s_{u0tc} \tag{32}$$

where $N_c$ = end bearing capacity factor and generally taken as 9 in clayey soils.

From Eqs. (23), (24), and (32), the time-dependent unit end resistance and end bearing capacity factor of driven piles in clay can be expressed as follows:

$$q_b(t) = N_c(t) s_{u0tc} \tag{33}$$

$$N_c(t) = N_c\frac{s_{utc}(t)}{s_{u0tc}} = \frac{p'(t)}{p'_0}\frac{N_c}{\mathrm{OCR}^{\Lambda}} \tag{34}$$

### Time-Dependent Total Axial Bearing Capacity

The axial capacity $Q_t$ of a single pile is composed of the shaft resistance $Q_s$ and base capacity $Q_b$; thus, the general equation for the time-dependent bearing capacity of driven piles can be determined by

$$Q_t(t) = Q_s(t) + Q_b(t) = \int_0^L C_s f_s(t)dz + A_b q_b(t) \tag{35}$$

where $L$ = pile length; $C_s$ = perimeter of the pile cross section; and $A_b$ = pile base area.

Interestingly, the long-term bearing capacity of a driven pile can be obtained from Eq. (35) if the time approaches infinite.

## Verification and Discussion

### Centrifuge Model Test

To verify the proposed analytical approach, an experimental program was undertaken in the centrifuge facility at Tongji University, Shanghai, China, to investigate the axial bearing performance of driven piles after installation. Three groups of centrifuge tests were conducted under a centrifugal acceleration of $50g$.

In the first group of tests, three miniature cone penetrometers with an effective length of 300 mm were used as model piles. The cone diameter of the penetrometer is 10 mm and the apex angle is 60°. The sleeve and pore-pressure transducer are located 60 mm and 10 mm above the cone tip, respectively. With these cone penetrometers, the unit end resistance and shaft resistance were measured by the electric strain gauge, and the dissipation of the excess pore pressure was tested by the pressure transducer connected to a porous filter element.

In the second group of tests, three aluminum alloy piles, each with radius of 6 mm, were used as model piles. In the third group of tests, the radius of the aluminum alloy model pile is 8 mm and three model piles were used. In the second and third group of tests, the total bearing capacity was measured by a pressure transducer, which was mounted between the top of the aluminum alloy pile and

the base of electrical motor jack through threaded caps. The electrical motor jack, provided with a step motor to control the rate of movement, was mounted at the top of the strongbox through two steel beams for pile installation and testing.

The silty clay, obtained from the fifth stratum in Shanghai City, was used in the tests. The soil sample was prepared using a vacuum stirring tank to provide relatively homogeneous slurry. The moisture content of the slurry was 1.5 times the liquid limit. Then, the slurry was poured into a strongbox with dimensions of $600 \times 400 \times 500$ mm and consolidated in the centrifuge at a centrifugal acceleration of 50$g$ for 12 h. Soil properties of the reconstituted samples are summarized in Table 1. The properties were mostly based on results from laboratory tests conducted on cylinder samples retrieved after completion of the centrifuge tests.

In each group of tests, the model pile was jacked into the soil sample at a constant rate of 50 mm/min in flight. This relatively fast rate was adopted to ensure the undrained conditions during pile installation (House et al. 2001). The instrumentation for measuring shaft and end resistance, as well as total bearing capacity, were reset to zero after pile installation to eliminate the effect of residual stresses. The axial compressive loading test was then conducted in flight using the electrical motor at a relatively slow constant rate of 5 mm/min to simulate the static loading tests. To avoid the reloading effects on the axial bearing capacity, each pile was tested only once. The detailed information of tested piles was summarized in terms of centrifuge scale in Table 2. The three piles in each group were positioned at the vertex of an equilateral triangle with a side length of 150 mm. Thus, the minimum distance between any two piles was 150 mm, and the minimum distance between the pile and the steel wall of the strongbox was 135 mm. This arrangement ensured minimum interaction and boundary effects (Hesham et al. 2000; Chow et al. 2014).

**Table 1.** Properties of the Soil Sample

| Soil property | Value |
|---|---|
| Effective unit weight [$\gamma'$ (kN/m$^3$)] | 8.75 |
| Effective internal friction angle [$\phi'$ (degrees)] | 30.0 |
| Slope of loading line ($\lambda$) | 0.11 |
| Slope of swelling line ($\kappa$) | 0.02 |
| Earth pressure coefficient at rest ($K_0$) | 0.55 |
| OCR | 1.0 |
| Horizontal coefficient of permeability [$k_h$ (m/s)] | $2.65 \times 10^{-7}$ |
| Void ratio ($e_0$) | 0.98 |

**Table 2.** Information of Tested Piles

| Pile number | Test group | Test time (min) | Diameter (mm) | Length (mm) | Embedded length (mm) |
|---|---|---|---|---|---|
| P1a | 1 | 5 | 10 | 300 | 250 |
| P1b | 1 | 10 | 10 | 300 | 250 |
| P1c | 1 | 60 | 10 | 300 | 250 |
| P2a | 2 | 5 | 12 | 280 | 200 |
| P2b | 2 | 10 | 12 | 280 | 200 |
| P2c | 2 | 60 | 12 | 280 | 200 |
| P3a | 3 | 5 | 16 | 280 | 200 |
| P3b | 3 | 10 | 16 | 280 | 200 |
| P3c | 3 | 60 | 16 | 280 | 200 |

### Test Results and Comparisons between Measured and Predicted Results

To assess the validity of the proposed theoretical approach, Figs. 5–12 present the results of the centrifuge model tests and the comparisons between the predicted and tested values. For clarity, the results are described in terms of prototype scales based on similarity conditions. Because all the load-settlement curves of the tested piles display an initial linear segment followed by a sudden large increase in settlement corresponding to little or no increase in the load, the pile capacity is defined as the load at the onset of the plunging failure in the following analysis.

Fig. 5 shows the dissipation of excess pore-water pressure at the depth of 12 m (24 mm in centrifuge model scale), which was measured from the pore-pressure transducer at the cone shoulder of the model pile P1c. The predicted curve from Eq. (14) is also presented for comparison. Fig. 5 shows that the predicted curve matches closely with the measured curve, which demonstrates that the generation and dissipation of the excess pore-water pressure can be properly predicted by the anisotropic cavity expansion solution and radial consolidation theory, respectively.

Fig. 6 shows the test results (from P1a, P1b, and P1c) of the mobilized pile shaft resistance, which were measured at the depth

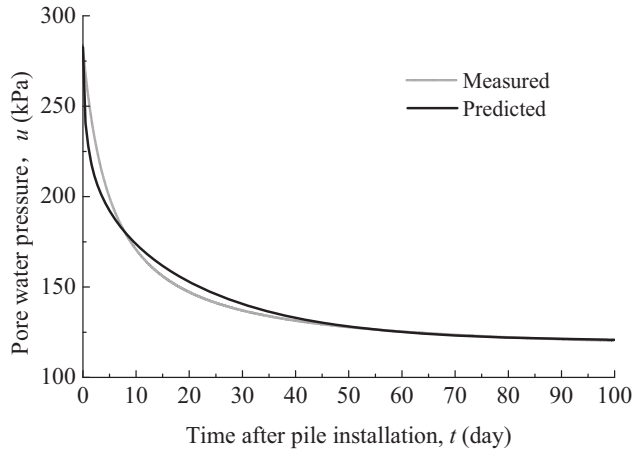


**Fig. 5.** Dissipation of excess pore-water pressure after pile installation

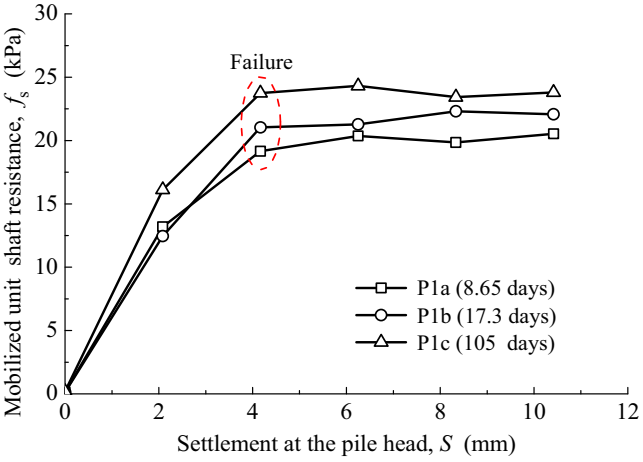


**Fig. 6.** Relationship between unit pile shaft resistance and pile head settlement at different reconsolidation times

of 9.5 m. Fig. 7 compares the time-dependent pile shaft resistance from Fig. 6 with the predictions calculated by Eqs. (22), (23), and (30). Fig. 6 shows that the pile shaft displayed an increase in resistance and a stiffer response with the passage of time. As seen in Fig. 7, the calculated results show a reasonable agreement with the measured values, which suggests that the proposed analytical approach can be applied to evaluate the time-dependent unit pile shaft resistance for a driven pile. It also can be seen in Fig. 7 that the unit shaft resistance increases rapidly within 5 days after pile installation and then increases slowly with time. Sixty days after the pile installation, the unit shaft resistance increases little with time and gradually reaches a constant value. Because the effective stress and the strength of the soil increase with dissipation of the excess pore-water pressure, the variation of the shaft resistance after pile installation can be explained by referring to Fig. 5.

The mobilized unit pile end resistance of P1a, P1b, and P1c, measured at the depth of 12.5 m, is shown in Fig. 8. The time-dependent unit pile end resistances from Fig. 8 are compared with the predictions calculated by Eqs. (22), (23), (33), and (34) in Fig. 9. As expected, Fig. 8 shows that the measured pile end resistance also increased with the passage of time. It can be seen in Fig. 9 that

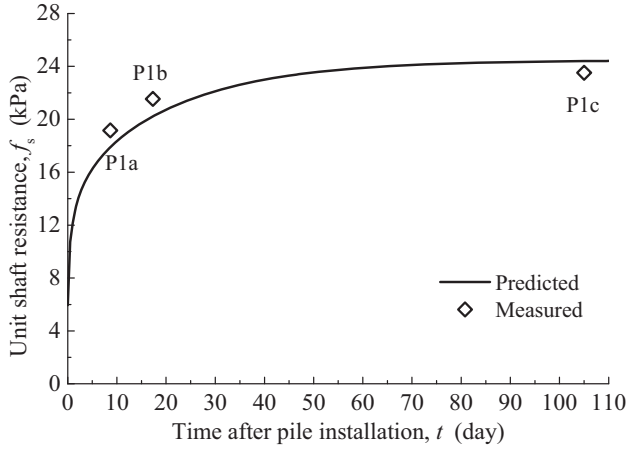


**Fig. 7.** Comparisons between predicted and measured values of the unit ultimate pile shaft resistance

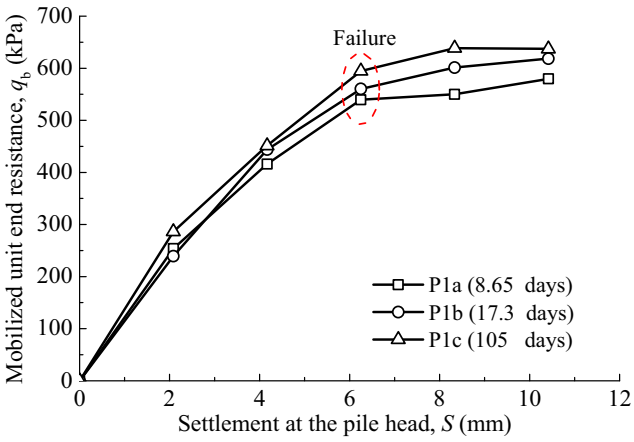


**Fig. 8.** Relationship between unit pile end resistance and pile head settlement at different reconsolidation times

the predictions yield a satisfactory agreement with the predicted values. In addition, it also can be observed from Fig. 9 that the pile end resistance increases rapidly after pile installation. About 90% of the change of the unit pile shaft resistance takes place only within 5.5 days after pile installation, and the increase of the unit pile end resistance is not obvious later.

The increases in normalized unit shaft resistance $f_s(t)/f_{s,t=\infty}$ and end resistance $q_b(t)/q_{b,t=\infty}$, along with the dissipation of the normalized excess pore-water pressure $\Delta u(t)/\Delta u_{t=0}$, obtained from the proposed theoretical approach and the first group tests, are comprehensively compared in Fig. 10. As seen in the figure, the pile shaft and pile end resistances increase with the dissipation of the excess pore-water pressure until they reach constant values. The gain in the resistance of pile shaft and end is directly related to the dissipation of the excess pore pressure. In addition, Fig. 10 shows that the pile end resistance increases more rapidly than the pile shaft resistance after pile installation. This is because the excess pore-water pressure dissipates faster around the pile tip due to the higher hydraulic gradient developed around the pile tip during pile installation. This phenomenon was also observed in the field test and demonstrated by Roy et al. (1981).

The results of the second and third group tests are presented in the form of load-settlement curves in Fig. 11, which shows that the total capacity increases substantially with time after pile installation. The increase in total bearing capacity is more apparent for the pile with a larger diameter. The total bearing capacity of the pile with a diameter of 0.6 m (12 mm in centrifuge model scale) increased 18.9% from 320.2 kN 8.65 days after pile installation to 394.6 kN 105 days after pile installation. For the pile with a diameter of 0.8 m (16 mm in centrifuge model scale), the total bearing capacity increased 23.0% from 447.7 kN 8.65 days after pile installation to 581.1 kN 105 days after pile installation.

Fig. 12 compares the change of the total bearing capacity measured from the second and third groups of tests (Fig. 11) with the calculated results from Eq. (35). It shows that there is a reasonable agreement between the measured and calculated values. Fig. 12 also shows that the total bearing capacity increases more rapidly for piles with a smaller diameter. For the pile with a diameter of 0.8 m, the total bearing capacity has increased by 50% during 3.5 days after pile installation and 90% during 42 days after pile installation. For the pile with a diameter of 0.6 m, the time required for a 50 and 90% increase in total bearing capacity are 2.2 and 33 days, respectively. The main reason for this phenomenon is that the drainage paths are larger for piles

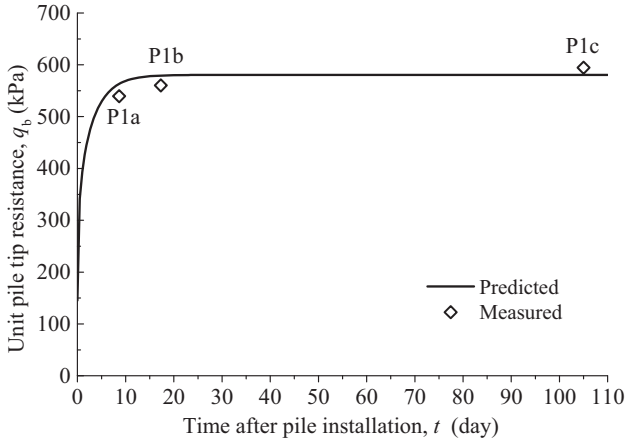


**Fig. 9.** Comparisons between predicted and test values of the unit ultimate pile end resistance

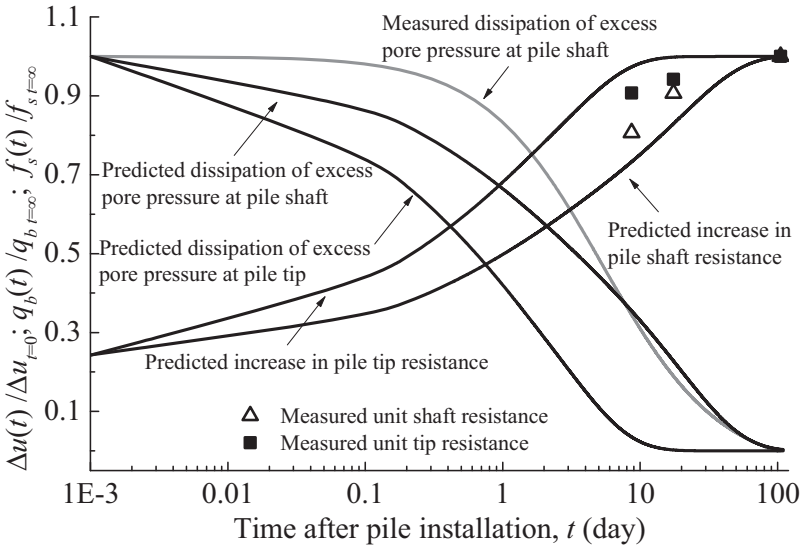


**Fig. 10.** Increase in normalized unit pile shaft and end bearing resistances and dissipation of normalized pore-water pressure with reconsolidated times

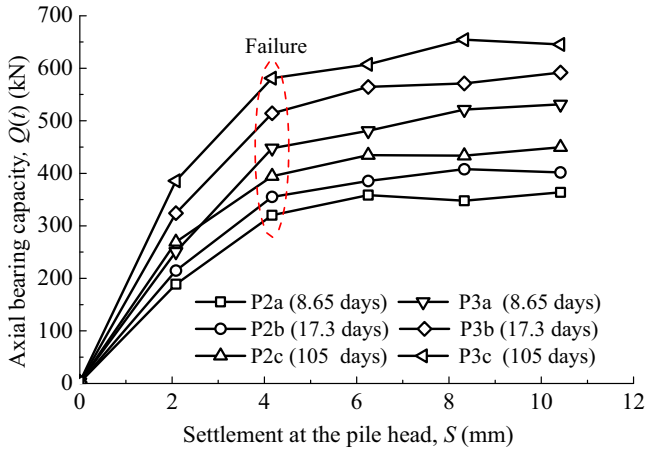


**Fig. 11.** Relationship between total bearing capacity and pile head settlement at different reconsolidation times

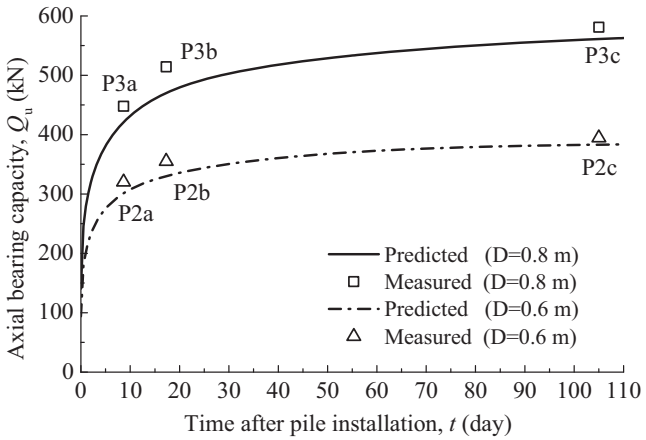


**Fig. 12.** Comparisons between predicted and measured values of pile bearing capacity at different reconsolidation times

with larger diameters, and the dissipation of the excess pore-water pressure primarily depends on the drainage path when the properties of the surrounding soil are the same.

The proposed approach in this paper is based on the undrained assumption for the pile installation process. However, the excess pore water generated by pile jacking dissipates inevitably during pile installation. Hence, the proposed solution may underestimate the axial bearing capacity immediately after pile installation. Nevertheless, the excess pore water dissipates at a relatively slow rate for a certain time after pile installation, so the proposed theoretical approach can reasonably predict the time-dependent bearing capacity beyond a certain time (e.g., 7 days in this study) after pile installation, especially for the long-term bearing capacity. Additionally, the effects of pile length and residual stress on the time-dependent bearing capacity are beyond the scope of the research in this paper; thus, these effects have not been considered in the presented theoretical approach.

## Pile Shaft and End Resistance Factors for Soils with Different Stress Histories

Most of the existing methods indirectly estimate the effect of stress history on resistance factors through the in situ undrained strength (Weltman and Healy 1978; Kulhawy and Jackson 1989). However, the undrained shear strength is a variable that depends on the friction angle, plastic volumetric strain ratio, OCR, effective stress, and the type of test. Therefore, it is rational and better to analyze the effect of stress history in terms of the OCR and the at-rest lateral earth pressure coefficient directly, which has the advantage of being independent of other irrelevant factors. In this section, some results for the time-dependent resistance factors with different OCRs are presented. Four different values of OCR = 1.1, 3, 6, and 10 are adopted to investigate the impact of the stress history on the resistance factors. The value of $K_0$ is approximated by the following expression (Mayne and Kulhawy 1982):

$$K_0 = (1 - \sin\phi')\mathrm{OCR}^{\sin\phi'} \quad (36)$$

Note that the values of other soil parameters used for analysis are the same as those listed in Table 1. Given that the rate of consolidation is affected by the coefficient of consolidation $C_h$ and the radius of the pile $r_d$, a suitable normalized time factor $T$ ($= C_h t/r_d^2$) is adopted in the following figures to facilitate its use for any values of $C_h$ and $r_d$.

Figs. 13 and 14 show the variation of the pile shaft and end resistance factors, respectively, with the normalized time factor for different values of OCR. The figures show that the rate of increase in the pile shaft and end resistances increases with OCR. This demonstrates that the time required for complete gain in total bearing capacity is shorter in soils with higher OCRs. It should be emphasized that although the permeability is generally smaller for soils with larger values of OCR, the difference in permeability will diminish after pile installation due to remolding effects. Hence, the primary reason for the higher rate of increase in the pile shaft and end resistances in the soil with larger OCR is that a higher gradient of the excess pore-water pressure occurs during the pile installation, which leads to quicker dissipation of the excess pore-water pressure. It is also interesting to note in Fig. 13 that both the long-term pile shaft and end resistance factors decrease as OCR increases, which agrees well with the variation given by previous empirical approaches (McClelland 1974; Randolph 2003). The reason for this phenomenon can be attributed to the remolding effects caused by pile installation, which can be well explained by Eqs. (22) and (23) presented in this paper.

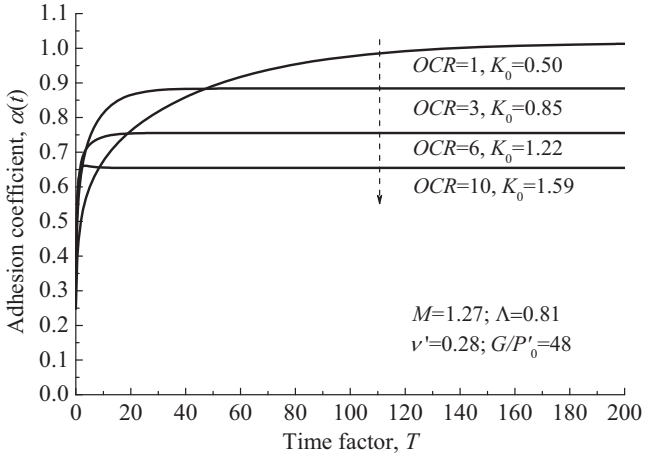


**Fig. 13.** Variation of pile shaft bearing capacity factors with time factors for different OCRs

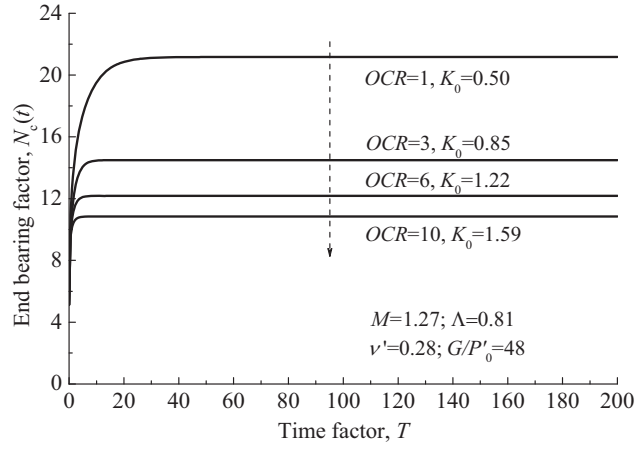


**Fig. 14.** Variation of pile end bearing capacity factors with time factors for different OCRs

## Summary and Conclusions

Dissipation of the excess pore-water pressure induced by pile installation depends to a great extent on the permeability coefficient and drainage path. Any specific time for a loading test might not be enough for the excess pore-water pressure to dissipate. Therefore, it is rational and necessary to develop a theoretical base that can properly consider the effect of time on the capacity for driven piles in various clay soils. In this paper, a total stress method-based analytical approach was developed to evaluate the time-dependent bearing capacity of a driven pile in clayey soils. Three groups of centrifuge model tests were performed to verify the validity of the proposed method. The present approach was applied to predict the test results and analyze the effects of in situ stress history on the pile shaft and end resistance factors. The main conclusions can be summarized as follows:

1. The proposed theoretical approach can be applied to evaluate the time-dependent bearing capacity of a driven pile in clayey soils. Comparisons between the predictions and the centrifuge model test results show a satisfactory agreement.
2. After pile installation, the increases in pile shaft and end resistance are directly related to the dissipation of the excess pore pressure. The increase in the end resistance is faster than the increase in the shaft resistance due to the higher excess pore pressure developed around the pile tip.
3. The predicted and test results show that the total bearing capacity increases substantially with time after pile installation. The pile diameter has a pronounced effect on the time-dependent bearing capacity. For the pile with a larger diameter, the increase in the total bearing capacity is more apparent, but the increase rate is slower.
4. The stress history has a pronounced effect on the time-dependent bearing capacity of driven piles. The time required for complete gain in total bearing capacity decreases with increasing OCR. The long-term bearing capacity factors for the pile shaft and end decreases with an increase in OCR.

## Acknowledgments

The authors are grateful for the support provided by the National Natural Science Foundation of China (Grant 41272288) for this research work. The anonymous reviewers' comments have improved the quality of this paper and are also greatly acknowledged.

## References

Abu-Farsakh, M., Rosti, F., and Souri, A. (2015). "Evaluating pile installation and subsequent thixotropic and consolidation setup by numerical simulation for full-scale pile load tests." *Can. Geotech. J.*, 52(11), 1734–1746.

Basu, P., Prezzi, M., Salgado, R., and Chakraborty, T. (2014). "Shaft resistance and setup factors for piles jacked in clay." *J. Geotech. Geoenviron. Eng.*, 10.1061/(ASCE)GT.1943-5606.0001018, 04013026.
Bond, A. J., and Jardine, R. J. (1991). "Effects of installing displacement piles in a high OCR clay." *Géotechnique*, 41(3), 341–363.
Butterfield, R., and Banerjee, P. K. (1970). "The effect of pore water pressures on the ultimate bearing capacity of driven piles." *Proc., 2nd South East Asian Conf. on Soil Engineering*, Bangkok, Thailand, 385–394.
Cao, L. F., Teh, C. I., and Chang, M. F. (2001). "Undrained cavity expansion in modified Cam clay I: Theoretical analysis." *Géotechnique*, 51(4), 323–334.
Chakraborty, D., and Kumar, J. (2013). "Bearing capacity of piles in soft Clay underlaid by cohesive frictional soil." *Int. J. Geomech.*, 10.1061/(ASCE)GM.1943-5622.0000211, 311–317.
Chow, S. H., Loughlin, C. D., and Randolph, M. F. (2014). "Soil strength estimation and pore pressure dissipation for free-fall piezocone in soft clay." *Géotechnique*, 64(10), 817–827.
Coop, M. R., and Wroth, C. P. (1990). "Discussion of M. R. Coop and C. P. Wroth 1989: Field studies of an instrumented model pile in clay." *Géotechnique*, 40(4), 669–672.
El Naggar, M. H., and Novak, M. (1992). "Analytical model for an innovative pile test." *Can. Geotech. J.*, 29(4), 569–579.
Elsherbiny, Z., and El Naggar, M. H. (2013). "Axial compressive capacity of helical piles from field tests and numerical study." *Can. Geotech. J.*, 50(12), 1191–1203.
Eslami, A., and Fellenius, B. H. (1997). "Pile capacity by direct CPT and CPTu methods applied to 102 case histories." *Can. Geotech. J.*, 34(6), 886–904.
Fakharian, K., Meskar, M., and Mohammadlou, A. S. (2014). "Effect of surcharge pressure on pile static axial load test results." *Int. J. Geomech.*, 10.1061/(ASCE)GM.1943-5622.0000310, 04014024.
Guo, W. D. (2000). "Visco-elastic consolidation subsequent to pile installation." *Comput. Geotech.*, 26(2), 113–144.
Hesham, M., Naggar, E., and Sakr, M. (2000). "Evaluation of axial performance of tapered piles from centrifuge tests." *Can. Geotech. J.*, 37(6), 1295–1308.
House, A. R., Oliveira, J. R. M. S., and Randolph, M. F. (2001). "Evaluating the coefficient of consolidation using penetration tests." *Int. J. Phys. Modell. Geotech.*, 1(3), 17–25.
Konrad, J. M., and Roy, M. (1987). "Bearing capacity of friction piles in marine clay." *Géotechnique*, 37(2), 163–175.
Kulhawy, F. H., and Jackson, C. S. (1989). "Some observations on undrained side resistance of drilled shafts." *Current principles and practices, Foundation Engineering Congress*, 2, ASCE, Reston, VA, 1011–1025.
Lehane, B. M., and Jardine, R. J. (1994). "Displacement pile behaviour in a soft marine clay." *Can. Geotech. J.*, 31(2), 181–191.
Li, L., Li, J. P., and Sun, D. A. (2016). "Anisotropically elasto-plastic solution to undrained cylindrical cavity expansion in $K_0$-consolidated clay." *Comput. Geotech.*, 73, 83–90.
Livneh, B., and El Naggar, M. H. (2008). "Axial testing and numerical modeling of square shaft helical piles under compressive and tensile loading." *Can. Geotech. J.*, 45(8), 1142–1155.
Mabsout, M. E., and Sadek, S. (2003). "A study of the effect of driving on pre-bored piles." *Int. J. Numer. Anal. Methods Geomech.*, 27(2), 133–146.
Matsuoka, H., and Sun, D. A. (2006). *The SMP concept-based 3D constitutive models for geomaterial*, Taylor & Francis, London.
Matsuoka, H., Yao, Y. P., and Sun, D. A. (1999). "The Cam-clay model revised by the SMP criterion." *Soils Found.*, 39(1), 81–95.
Mayne, P. W., and Kulhawy, F. H. (1982). "K0-OCR relationships in soils." *J. Geotech. Eng. Div.*, 108(6), 851–872.
McClelland, B. (1974). "Design of deep penetration piles for ocean structures." *J. Geotech. Geoenviron. Eng. Div.*, 100, 709–747.
Mohamed, E., and El Naggar, M. H. (2015). "Axial compressive response of large-capacity helical and driven steel piles in cohesive soil." *Can. Geotech. J.*, 52(2), 224–243.
Ng, K., Suleiman, M., and Sritharan, S. (2013). "Pile setup in cohesive soil. II: Analytical quantifications and design recommendations." *J. Geotech. Geoenviron. Eng.*, 10.1061/(ASCE)GT.1943-5606.0000753, 210–222.
Pestana, J., Hunt, C., and Bray, J. (2002). "Soil deformation and excess pore pressure field around a closed-ended pile." *J. Geotech. Geoenviron. Eng.*, 10.1061/(ASCE)1090-0241(2002)128:1(1), 1–12.
Qi, C., Liu, G., Wang, Y., and Deng, Y. (2015). "A design method for plastic tube cast-in-place concrete pile considering cavity contraction and its validation." *Comput. Geotech.*, 69, 262–271.
Randolph, M. F. (2003). "Science and empiricism in pile foundation design." *Géotechnique*, 53(10), 847–875.
Randolph, M. F., and Wroth, C. P. (1979). "An analytical solution for the consolidation around a driven pile." *Int. J. Numer. Anal. Methods Geomech.*, 3(3), 217–229.
Randolph, M. F., and Wroth, C. P. (1981). "Application of the failure state in undrained simple shear to the shaft capacity of driven piles." *Géotechnique*, 31(1), 143–157.
Roy, M., Blanchet, R., Tavenas, F., and Rochelle, P. L. (1981). "Behaviour of a sensitive clay during pile driving." *Can. Geotech. J.*, 18(1), 67–85.
Sekiguchi, H., and Ohta, H. (1977). "Induced anisotropy and time dependency in clays." *Proc., 9th ICSMFE*, Japanese Society of Soil Mechanics and Foundation Engineering, Tokyo, 229–238.
Skov, R., and Denver, H. (1988). "Time dependence of bearing capacity of piles." *Proc., 3rd Int. Conf. Application of Stress-Wave Theory to Piles*, B. H. Fellenius, ed., BiTech, Ottawa, 879–888.
Veiskarami, M., Eslami, A., and Kumar, J. (2011). "End-bearing capacity of driven piles in sand using the stress characteristics method: Analysis and implementation." *Can. Geotech. J.*, 48(10), 1570–1586.
Vesic, A. S. (1973). "Analysis of ultimate loads of shallow foundations." *J. Soil Mech. Found. Div.*, 99(1), 45–73.
Weltman, A. J., and Healy, P. R. (1978). "Piling in boulder clay and other glacial tills." *Rep. PG5*, Construction Industry Research and Information Association, London.
Yang, L., and Liang, R. (2006). "Incorporating set-up into reliability-based design of driven piles in clay." *Can. Geotech. J.*, 43(9), 946–955.
Yu, H. S. (2000). *Cavity expansion methods in geomechanics*, Kluwer Academic, Dordrecht, Netherlands.